Results in Physics 8 (2018) 172–179

Contents lists available at ScienceDirect

Results in Physics

journal homepage: www.journals.elsevier.com/results-in-physics

Surface coverage and corrosion inhibition effect of *Rosmarinus officinalis* and zinc oxide on the electrochemical performance of low carbon steel in dilute acid solutions

Roland Tolulope Loto

Department of Mechanical Engineering, Covenant University, Ota, Ogun State, Nigeria

ARTICLE INFO

Article history:
Received 26 October 2017
Received in revised form 22 November 2017
Accepted 2 December 2017
Available online 6 December 2017

Keywords:
Corrosion
Inhibitor
Adsorption
Steel
Acid

ABSTRACT

Electrochemical analysis of the corrosion inhibition and surface protection properties of the combined admixture of *Rosmarinus officinalis* and zinc oxide on low carbon steel in 1 M HCl and H_2SO_4 solution was studied by potentiodynamic polarization, open circuit potential measurement, optical microscopy and ATR-FTIR spectroscopy. Results obtained confirmed the compound to be more effective in HCl solution, with optimal inhibition efficiencies of 93.26% in HCl and 87.7% in H_2SO_4 acid solutions with mixed type inhibition behavior in both acids. The compound shifts the corrosion potential values of the steel cathodically in HCl and anodically in H_2SO_4 signifying specific corrosion inhibition behavior without applied potential. Identified functional groups of alcohols, phenols, 1°, 2° amines, amides, carbonyls (general), esters, saturated aliphatic, carboxylic acids, ethers, aliphatic amines, alkenes, aromatics, alkyl halides and alkynes within the compound completely adsorbed onto the steel forming a protective covering. Thermodynamic calculations showed physisorption molecular interaction with the steel's surface according to Langmuir and Frumkin adsorption isotherms. Optical microscopy images of the inhibited and uninhibited steels contrast each other with steel specimens from HCl solution showing a better morphology.

Introduction

Corrosion reaction mechanisms are responsible for damages to metallic structures leading to major industrial accidents, plant shut downs and downtime, and costly replacement of metallic parts of equipment. Use of chemical compounds known as corrosion inhibitors have seen increased application in cooling systems, oil refineries, pipelines, chemical processing plants, boilers and water processing, paints, pigments, lubricants etc. among various other methods of corrosion prevention due to their relatively lower cost and ease of use [1,2]. Current report shows that the U.S. demand for corrosion inhibitors will rise to 4.1% (USD$ 2.5 billion) in 2017 [3]. However, the negative effects and toxicity of some corrosion inhibitors especially those of inorganic origin such as chromates, nitrates, phosphates etc. on the environment and human health necessitates the need for environmentally sustainable replacements [4,5]. Some inorganic compounds such as molybdates, tungstates, zinc phosphomolybdate, lanthanide compounds etc. exhibits good eco-friendly attributes but are quite expensive. Study of molecules of natural or organic origin exhibiting strong adsorption or protective film onto/over metallic surfaces in corrosive media are one of the most promising research areas toward the development of sustainable inhibiting compounds. Adsorption by organic compounds with multi-functional groups within their molecular structure consisting of heteroatoms, triple bonds or aromatic rings enhances the adsorption process. This property coupled with the ability to effectively form a strong adherent film that hinders the diffusion and electrolytic transport of corrosive species onto the metal is an important characteristic necessary for effective corrosion inhibition [6–12]. Rosmarinus officinalis a green organic compound has been previously studied for its corrosion inhibition effect [13–23]. Previous research of Zinc oxide has shown that it has good corrosion inhibition and synergistic properties [24–27]. Zinc oxide is widely used in coatings and as an additive in rubbers [28,29]. In contribution to research on the use of eco-friendly compounds for corrosion inhibition, this research aims to study the combined inhibiting action and adsorption properties of *Rosmarinus officinalis* extracts and zinc oxide on the corrosion inhibition of low carbon steel in dilute HCl and H_2SO_4 acid media.

E-mail address: tolulope.loto@covenantuniversity.edu.ng

https://doi.org/10.1016/j.rinp.2017.12.003
2211-3797/

Experimental methods

Materials and preparation

Low carbon steel (LCS) rod (1 cm diameter) sourced from the open market has a nominal (wt%) composition presented in Table 1. The carbon steel was cut and sectioned with Clarke power hacksaw and ESM 700 excel shaping machine to give steel specimens with average length of 1 cm. The steel specimen surfaces were grinded with silicon carbide papers (80, 320, 600, 800 and 1000 grit), afterwards cleansed with deionized water and propanone, and kept in a desiccator for electrochemical test and corrosion potential measurement according to ASTM G1 – 03 [30].

Rosmarinus officinalis obtained from NOW Foods, USA with a purity of 100% was extracted through steam distillation from tops of plant. It is a golden, translucent, oily liquid with a molar mass (active groups) of 691.14 g/mol [31]. Zinc oxide obtained from the University of Lagos, Nigeria is a silvery white powder with a molar mass of 81.38 g/mol. The combined admixture of *Rosmarinus officinalis* and zinc oxide abbreviated as RSZ was prepared in molar concentrations of 6.47×10^3, 1.29×10^2, 1.94×10^2, 2.59×10^2, 3.24×10^2 3.88×10^2 in 200 mL of 1 M HCl and H_2SO_4 solution. The dilute acids were prepared from analar grade of the acids (37% HCl and 98% H_2SO_4) with deionized water.

Potentiodynamic polarization technique

Polarization measurements were carried out at ambient temperature 37 °C using a three electrode system and aerated glass cell containing 200 mL of the corrosive test solution connected to Digi-Ivy 2311 electrochemical workstation. LCS electrodes mounted in acrylic resin with an exposed surface area of 0.79 cm^2 were prepared according to ASTM G59-97 [32]. Polarization plots were obtained at a scan rate of 0.0015 V/s between potentials of −1 V and +1 V according to ASTM G102-89 [33]. A platinum rod was used as the counter electrode and a silver chloride electrode (Ag/AgCl) as the reference electrode. Corrosion current density (j_{cr}, A/cm^2) and corrosion potential (E_{cr}, V) values were obtained using the Tafel extrapolation method. The corrosion rate values of LCS (C_R) were calculated from the mathematical relationship;

$$C_R = \frac{0.00327 \times j_{cr} \times E_{qv}}{D} \quad (1)$$

D is the density in g/cm^3; E_{qv} is the sample equivalent weight in grams. 0.00327 is a constant for corrosion rate calculation in mm/y [34]. Inhibition efficiency values of RSZ, η (%) were calculated from corrosion rate results according to Eq. (2) below;

$$\eta_2 = \left[1 - \left(\frac{C_{R2}}{C_{R1}}\right)\right] \times 100 \quad (2)$$

C_{R1} is the corrosion rate of LCS without RSZ compound and C_{R2} represents the corrosion rates of LCS with RSZ compound at specific concentrations.

Open circuit potential (OCP) measurement

OCP measurements were obtained at a step potential of 0.05 V/s with two-electrode electrochemical cell consisting of Ag/AgCl reference electrode and resin mounted steel specimens (exposed surface of 0.79 cm^2) as the working electrode, connected to Digi-Ivy 2311 potentiostat according to ASTM G69 – 12 [35]. The electrodes were fully immersed in 200 mL of the test media at specific concentrations of 0% RSZ and 3% RSZ for 3000 s.

ATF-FTIR spectroscopy and optical microscopy characterization

RSZ/1 M HCl and H_2SO_4 solution (before and after the corrosion test) were exposed to specific range of infrared ray beams from Bruker Alpha FTIR spectrometer at wavelength range of 375–7500 cm^{-1} and resolution of 0.9 cm^{-1}. The transmittance and reflectance of the infrared beams at various frequencies were decoded and transformed into an FTIR absorption plot consisting of spectra peaks. The spectral pattern was evaluated and equated with FTIR absorption table to identify the functional groups responsible for corrosion inhibition. Images of the corroded and inhibited LCS surface morphologies from optical microscopy were analysed after the electrochemical test with Omax trinocular metallurgical microscope with the aid of ToupCam analytical software.

Results and discussion

Potentiodynamic polarization studies

The potentiodynamic polarization curves for RSZ inhibition on LCS in HCl and H_2SO_4 solution are depicted in Figs. 1 and 2. Results obtained are shown in Table 2. Differences in corrosion rate values between the inhibited (0.5%–3% RSZ) and uninhibited (0% RSZ) LCS specimens in both acids is due to the presence and corrosion

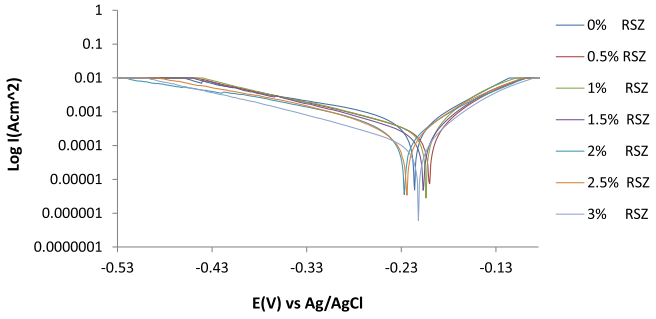

Fig. 1. Potentiodynamic polarization curves for LCS in (0–3% RSZ) 1 M HCl.

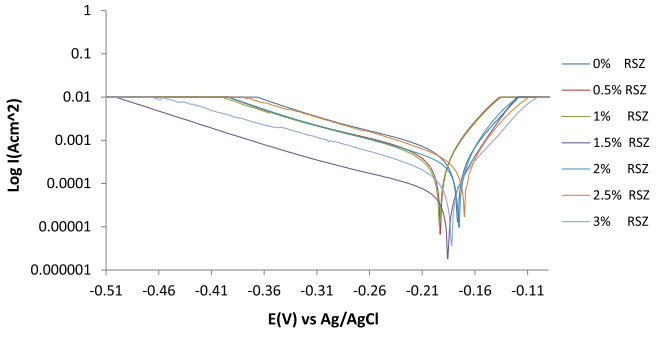

Fig. 2. Potentiodynamic polarization curves for LCS in (0–3% RSZ) 1 M H_2SO_4.

Table 1
Nominal Composition (wt%) of LCS.

Element Symbol	Si	S	Mn	C	P	C	Fe
% Composition	0.40	0.04	0.8	0.02	0.04	0.16	98.54

inhibition properties of RSZ compound. At 0% RSZ, LCS oxidizes in the acid solutions resulting in the formation of porous oxides on the steel's surface. Growth of oxide films accelerated faster in H_2SO_4 than in HCl leading to greater formation of pores and channels on the steel surface, resulting in higher corrosion rate value (Table 1). The higher corrosion rate H_2SO_4 than HCl acid is due to its ability of H_2SO_4 to completely ionize in the solution releasing two protons that strongly reacts with the steel surface compared to HCl which release only one proton. Corrosive anions of SO_4^{2-} and Cl^- within the acid solution aggravated the corrosion of the steel mainly due to depassivation effect in iron dissolution. The inhibition efficiency values show RSZ performed effectively, but relatively higher in HCl solution coupled with its lower corrosion current density.

Increase in RSZ concentration caused LCS corrosion potential values in HCl to shift in the cathodic direction after 1% RSZ due to the predominant influence of RSZ on the hydrogen evolution and oxygen reduction reactions of the steel through increase in surface impedance and selective precipitation on the steel surface. This observation is similar to the RSZ behavior in H_2SO_4 solution. The corrosion potential also shifted to cathodic values. These observations are possibly due to release of excess electrons which slows down the anodic reaction and speeds up the cathodic reaction mechanism. RSZ caused a decrease in the current densities, most likely due to the adsorption of the organic compounds at the active sites of the electrode surface. Zinc oxide component particles of RSZ provide corrosion protection through formation of a barrier between the acid solution and the ferrous metal surface. They have the property of keeping out moisture that accelerates the corrosion process. Zinc oxide being more electrochemically active than iron, serves as the anode for the steel in the acid solution preventing the formation of small anodic and cathodic sites on the metal surface. The inhibition mode of RSZ as earlier discussed has significant but limited influence on the Tafel slopes values after 0% RSZ suggesting that the inhibiting compound does actively participate in the corrosion mechanism [36]. This is further proven from the inhibition efficiency results, whereby its values were slightly influenced by changes in RSZ concentration. The maximum change in corrosion potential of LCS in HCl solution is 16 mV, while in H_2SO_4 the change in corrosion potential is 18 mV, thus RSZ is a mixed type inhibitor in both acid solution [37].

ATR-FTIR spectroscopy analysis

Functional groups and bond types within the molecular structure of RSZ compound responsible for molecular adsorption and corrosion inhibition of LCS surface in HCl and H_2SO_4 solution were identified as shown on Tables 3 and 4 after being matched with the FTIR Table [38,39]. The spectrum plots of the test solution from both acids before and after the corrosion test are shown in Fig. 3. Functional groups of alcohols, phenols, 1° and 2° amines, amides, carbonyls (general), esters, saturated aliphatic, carboxylic acids, ethers, aliphatic amines, alkenes, aromatics, alkyl halides, alkanes and alkynes within RSZ compound in HCl are shown in Table 3. Comparative observation of the calculated wavenumber of RSZ compound, before and after corrosion shows that most identified groups completely adsorb on LCS surface in HCl solution through surface coverage, inhibiting the corrosion. The bonds present within their molecular structure consisting of O—H stretch, H–bonded, N—H stretch, C=O stretch, C—O stretch, C—H wag (—CH_2-X), C—N stretch, =C—H bend, N—H wag, C—H "oop", C—Cl stretch, —C≡C—H, C—H bend, C—H stretch, C—C stretch (in–ring) and C—Br stretch are responsible for attachment through weak van der waals forces to the valence electron of LCS, inhibiting the oxidation of the steel. Partial adsorption of carboxylic acids, alkanes, alcohols, phenols, 1° and 2° amines and amides having C—H stretch, H–bonded, N—H stretch and O—H stretch bonds were also observed. Similar observation was also noted for RSZ adsorption and inhibition of LCS in H_2SO_4 solution (Table 4).

Adsorption isotherm

Adsorption mechanisms occur when liquid solute accumulates on solid surfaces, forming a molecular or atomic film. The inhibition mechanism of RSZ through adsorption on LCS surface was further investigated through adsorption isotherms models. The isotherms depict the phenomenon governing the retention of a substance from aqueous porous media to a solid-phase at constant temperature and pH [40,41]. Adsorption is a product of electrostatic attraction and/or covalent bonding between the valence electrons on metallic surfaces and hetero-atoms of RSZ compound, which involves the removal of water molecules and formation of a protective film. These mechanisms are complex and depend on the functional groups of the inhibiting compound, their ionization potential, corrosivity and pH of the acid solution. Its physicochemical parameters in addition to the underlying thermodynamic assumptions give invaluable information about the adsorption mechanism and surface properties as well as the degree of affinity of the adsorbents [42]. Langmuir and Frumkin adsorption isotherm gave the best fitting as shown from Figs. 4 and 5 according to the following equations.

Table 2
Potentiodynamic polarization result for LCS in 1 M HCl and H_2SO_4 solution (0%–3% RSZ) acid solution.

Sample	RSZ Conc. (%)	RSZ Conc. (M)	Corrosion Rate (mm/y)	RSZ Inhibition Efficiency (%)	Corrosion Current (A)	Corrosion Current Density (A/cm^2)	Corrosion Potential (V)	Polarization Resistance, R_p (Ω)	Cathodic Tafel Slope, B_c (V/dec)	Anodic Tafel Slope, B_a (V/dec)
HCl										
A	0	0	85.89	0	5.81E−03	7.40E−03	−0.216	34.89	−5.512	0.087
B	0.5	6.47E−03	8.37	90.26	5.66E−04	7.21E−04	−0.200	701.60	−7.241	0.168
C	1	1.29E−02	8.43	90.18	5.71E−04	7.27E−04	−0.204	854.94	−7.322	0.206
D	1.5	1.94E−02	7.68	91.06	5.20E−04	6.62E−04	−0.207	986.11	−8.060	0.216
E	2	2.59E−02	6.00	93.01	4.06E−04	5.17E−04	−0.227	808.86	−6.744	0.140
F	2.5	3.24E−02	5.92	93.11	4.01E−04	5.10E−04	−0.224	1159.29	−7.953	0.197
G	3	3.88E−02	5.79	93.26	3.92E−04	4.99E−04	−0.212	1006.11	−7.917	0.167
H_2SO_4										
A	0	0	120.23	0	8.14E−03	1.04E−02	−0.176	31.2	−6.106	0.108
B	0.5	6.47E−03	32.12	73.3	2.17E−03	2.77E−03	−0.193	404.6	−5.724	0.358
C	1	1.29E−02	28.47	76.3	1.93E−03	2.45E−03	−0.194	385.7	−6.323	0.307
D	1.5	1.94E−02	21.48	82.1	1.45E−03	1.85E−03	−0.186	812.6	−5.781	0.471
E	2	2.59E−02	16.89	86.0	1.14E−03	1.46E−03	−0.175	2185.2	−6.576	0.931
F	2.5	3.24E−02	14.60	87.9	9.88E−04	1.26E−03	−0.170	1723.5	−7.615	0.674
G	3	3.88E−02	14.75	87.7	9.98E−04	1.27E−03	−0.182	2028.4	−6.926	0.780

Table 3
ATR-FTIR spectroscopic data of frequencies and adsorption peaks of RSZ/1M HCl solution before and after LCS corrosion.

Theoretical wavenumber (cm^{-1})	Calculated Wavenumber, Before Corrosion (cm^{-1})	Calculated Wavenumber, After Corrosion (cm^{-1})	Bond	Functional group
3400–3250 3500–3200	3344.97	3226.17	O—H stretch, H–bonded, N—H stretch	alcohols, phenols, 1°, 2° amines, amides
3300–2500 3000–2850	2954.80, 2853.98	2922.54, 2853.30	O—H stretch, C—H stretch	carboxylic acids, alkanes
3300–2500 3000–2850	2921.98	–	O—H stretch, C—H stretch	carboxylic acids, alkanes
1760–1665 1760–1690 1750–1735	1746.92, 1735.90	–	C=O stretch	carbonyls (general), esters, saturated aliphatic
1550–1475	1541.90	–	C—C stretch (in-ring), C—H bend	aromatics, alkanes
1320–1000 1300–1150 1250–1020	1214.97, 1166.83, 1052.43	–	C—O stretch, C—H wag ($-CH_2X$), C—N stretch	alcohols, carboxylic acids, esters, ethers, alkyl halides, aliphatic amines
1000–650 910–665 900–675 850–550	985.27, 885.34, 842.82, 721.2	–	=C—H bend, N—H wag, C—H "oop", C—Cl stretch	alkenes, 1°, 2° amines, aromatics, alkyl halides
850–550 700–610 690–515	625.91	–	C—Cl stretch, —C≡C—H: C—H bend, C—Br stretch	alkyl halides, alkynes,

Table 4
ATR-FTIR spectroscopic data of frequencies and adsorption peaks of RSZ/1M H_2SO_4 solution before and after LCS corrosion.

Theoretical wavenumber (cm^{-1})	Calculated Wavenumber, Before Corrosion (cm^{-1})	Calculated Wavenumber, After Corrosion (cm^{-1})	Bond	Functional group
3300–2500 3000–2850	2921.56, 2853.56	2920.69, 2852.42	O—H stretch, C—H stretch	carboxylic acids, alkanes
1760–1665 1760–1690 1750–1735	1747.46	1634.55	C=O stretch	carbonyls (general), carboxylic acids, esters, saturated aliphatic
1500–1400 1470–1450	1461.75	1460.42	C—C stretch (in–ring), C—H bend	aromatics, alkanes
1320–1000 1300–1150 1250–1020	1214.77, 1166.76, 1079.54, 1052.22, 1016.88	–	C—O stretch, C—H wag ($-CH_2X$), C—N stretch	alcohols, carboxylic acids, esters, ethers, alkyl halides, aliphatic amines
1000–650 910–665 900–675 850–550	985.37, 885.96, 843.50, 787.28	–	=C—H bend, N—H wag, C—H "oop", C—Cl stretch	alkenes, 1°, 2° amines, aromatics, alkyl halides
725–720	722.96	721.95	C—H rock	alkanes

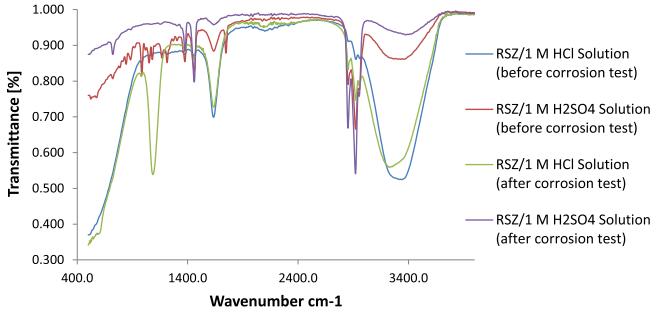

Fig. 3. ATR-FTIR spectra of RSZ compound in 1 M HCl and H_2SO_4 solution before and after LCS corrosion.

Plots of $\frac{C_{RSZ}}{\theta}$ vs C_{RSZ} perfectly fits with Langmuir isotherm [Fig. 4a and (b)], with a correlation coefficient of 0.9998 in HCl solution and 0.9988 in H_2SO_4 according to the equation below.

$$\theta = \left[\frac{K_{ads}C_{RSZ}}{1 + K_{ads}C_{RSZ}}\right] \quad (3)$$

where θ is the extent of RSZ adsorbed per unit weight on LCS surface at equilibrium, C_{RSZ} is RSZ concentration and K_{ads} is the equilibrium constant of the adsorption mechanism. Langmuir isotherm suggests monolayer layer adsorption at specific reaction sites on the steel's surfaces. The adsorptions are identical, equivalent and no lateral interaction between the adsorbed molecules exists [43].

The Frumkin adsorption isotherm suggests the steel surface is heterogeneous i.e. lateral interaction effect is not negligible. The equation is as follows [44]:

$$\theta/1-\theta = Kce^{2\alpha\theta} \quad (4)$$

rearranging we have

$$\log[\theta/(1-\theta)c] = 2.303\log K + 2\alpha\theta \quad (5)$$

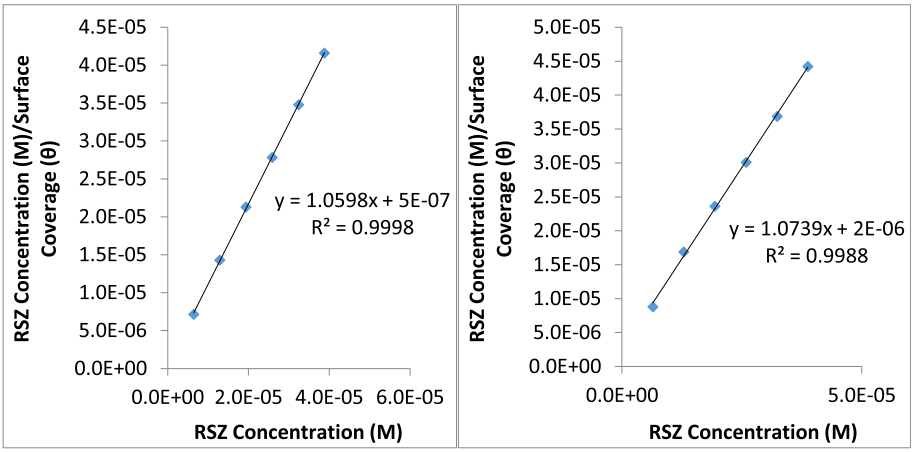

Fig. 4. Langmuir plot of $\frac{c}{\theta}$ versus RSZ concentration (a) in 1 M HCl, (b) in 1 M H_2SO_4.

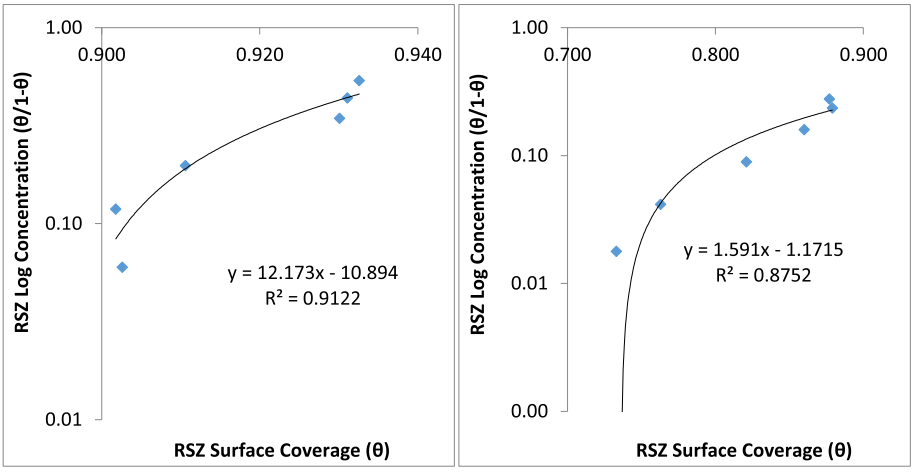

Fig. 5. Frumkin isotherm plot of $\log[\theta/(1-\theta)c]$ versus θ (a) in 1 M HCl, (b) in 1 M H_2SO_4.

where α is the interaction parameter describing the interaction in adsorbed layer. It is calculated from the slope of the Frumkin isotherm. Taking into account, the attraction ($\alpha > 0$) or repulsion ($\alpha < 0$) between the adsorbed species. If $\alpha = 0$ (no interaction), the isotherm becomes equivalent to the Langmuir isotherm. For +ve α, adsorption energy increases with θ whereas for negative α adsorption energy decreases with θ. K is the adsorption-desorption constant. Plots of $\log[\theta/(1-\theta)c]$ versus θ in Fig. 5(a) and (b) showed a correlation coefficient of 0.9122 in HCl solution and 0.8752 in H_2SO_4.

Thermodynamics of the corrosion inhibition mechanism

The strength and type of adsorption of RSZ on LCS was determined from the thermodynamics of the inhibition mechanism through the equilibrium constant of adsorption from the Langmuir isotherm due to its correlation coefficient closest unity. Calculated results of Gibbs free energy of adsorption is shown in Tables 5 and 6, from the mathematical relationship below [45].

$$\Delta G_{ads} = -2.303RT\log[55.5K_{ads}] \quad (6)$$

where 55.5 is the molar concentration of water in the solution, R is the universal gas constant, T is the absolute temperature and K_{ads} is the equilibrium constant of adsorption. K_{ads} is related to surface coverage (θ) from the Langmuir equation.

Negative values of ΔG^o_{ads} show the adsorption reaction mechanisms is spontaneous and stable with the lowest of ΔG^o_{ads} value of -24.52 KJ mol^{-1} at 3.88×10^2M and the highest ΔG^o_{ads} value of -27.96 KJ mol^{-1} at 6.47×10^3M on LCS surface in HCl. The lowest and highest values in H_2SO_4 are -22.87 KJ mol^{-1} at 3.88×10^2M

Table 5
Results for Gibbs free energy (ΔG^o_{ads}), surface coverage (θ) and equilibrium constant of adsorption (K_{ads}) for RSZ adsorption on LCS in 1 M HCl.

LCS Specimen	RSZ Concentration (M)	Surface Coverage (θ)	Equilibrium Constant of adsorption (K_{ads})	Gibbs Free Energy, ΔG (KJ mol^{-1})
A	0	0	0	0
B	6.47E−03	0.903	1432.3	−27.96
C	1.29E−02	0.902	711.9	−26.23
D	1.94E−02	0.911	525.0	−25.47
E	2.59E−02	0.930	513.8	−25.42
F	3.24E−02	0.931	417.1	−24.90
G	3.88E−02	0.933	356.6	−24.52

Table 6
Results for Gibbs free energy (ΔG^{o}_{ads}), surface coverage (θ) and equilibrium constant of adsorption (K_{ads}) for RSZ adsorption on LCS in 1 M H_2SO_4.

Specimen	RSZ Concentration (M)	Surface Coverage (θ)	Equilibrium Constant of adsorption (K_{ads})	Gibbs Free Energy, ΔG (KJ mol^{-1})
A	0	0	0	0
B	6.47E−03	0.733	424.3	−24.95
C	1.29E−02	0.763	249.6	−23.63
D	1.94E−02	0.821	236.4	−23.50
E	2.59E−02	0.860	237.2	−23.50
F	3.24E−02	0.879	224.2	−23.37
G	3.88E−02	0.877	183.8	−22.87

and the lowest value of −24.95 KJ mol^{-1} at 6.47 × 10^3M. The ΔG^{o}_{ads} values in both acid solutions show physisorption reaction i.e. physical interaction of RSZ molecules through Vander Waals forces on the steel's surface [46,47]. This shows that surface coverage with minimal covalent/electrostatic interaction according to Langmuir and Frumkin adsorption isotherm is responsible for corrosion inhibition of LCS. The values are generally higher for LCS in HCl compared to H_2SO_4, due to the higher corrosion rate of LCS in H_2SO_4.

Open circuit potential measurement

Variation of corrosion potential with exposure time for inhibited and uninhibited LCS in 1 M HCl and H_2SO_4 solution for 3000 s is shown in Fig. 6. Corrosion potential values for uninhibited LCS in HCl solution started at $-0.192V_{Ag/AgCl}$ at 0 s and progressively increased to $-0.180V_{Ag/AgCl}$ at 609 s after which the values remained generally constant till 3000 s as a result of polarization of LCS surface in the presence of Cl^- ions such that anodic reactions predominate before stability. This observation contrasts the behavior of LCS in H_2SO_4; the corrosion potential shifts from $-0.146V_{Ag/AgCl}$ at 0 s to $-0.177V_{Ag/AgCl}$ at 972 s at which it stabilizes due to domination of the cathodic reaction mechanism. The reaction involves reduction of hydrogen ions and oxygen molecules which adsorbs on the metal surface. Addition of RSZ compound to both solutions shifts the corrosion potential of LCS in opposite directions. The corrosion potential in HCl stabilizes at 635 s/$-0.192V_{Ag/AgCl}$ till the end of the exposure hours due to cathodic inhibition effect of RSZ which permeates especially on actives sites responsible for metal oxidation, hence cathodic shift in corrosion potential. In H_2SO_4 solution RSZ stifles the anodic reaction mechanism over the steel surface resulting in anodic shift of LCS corrosion potential which stabilizes at 803 s/$-0.160V_{Ag/AgCl}$ however potential transients occurred from 0 s/$-0.135V_{Ag/AgCl}$ to 1018 s/$-0.160V_{Ag/AgCl}$ probably as a result of the gradual coverage and stability of RSZ over the steel surface. Observation of the inhibited corrosion potentials in comparison to the uninhibited potentials shows the visible electrochemical influence of RSZ on the redox electrochemical reaction of LCS in HCl and H_2SO_4 solution.

Optical microscopy analysis

Micro-analytical images of LCS before and after the corrosion test, with and without RSZ compound from HCl and H_2SO_4 solution are shown in Figs. 7a–9b. Fig. 7(a) and (b) shows the images of the untested steel with visible lines due to machining and metallographic preparation. The corroded steel surface from HCl and H_2SO_4 solution [Figs. 8(a) and 9(a)] shows a badly deteriorated morphology with visible macro and micro pits. The extent of deterioration tends to be higher on the steel specimen from HCl due to electrochemical action of Cl^- ions. The Cl^- ions significantly aggravates the conditions for formation and growth of the pits through an autocatalytic process. The special chemistry within the pit electrolyte created in HCl solution contrast the pit created from H_2SO_4 due to the presence of SO_4^{2-}, as a result LCS specimen from HCl tends to have fewer but larger pits compared to specimens from H_2SO_4 which has more but smaller pits.

Addition of RSZ compound to both acid solutions with LCS [Figs. 8(b) and 9(b)] changes the dynamics of the electrochemical process, hence the morphology of LCS specimens. The morphology of LCS from HCl mildly deteriorated compared to the image from H_2SO_4 due to more effective inhibiting action of RSZ in HCl as confirmed from polarization test results. The serrated edges are still visible in Fig. 8(b) as a result of adsorption of RSZ cations onto the steel which inhibits the diffusion and electrolytic transport of Cl^- ions. The higher electronegativity of Cl^- ions compared to SO_4^{2-} ions enables stronger electrostatic attraction onto LCS surface, specifically attachment onto the valence electrons of the steel which prevents oxidation of the steel. The inhibited LCS surface [Fig. 9(b)] presents a significantly better morphology than the corroded surface [Fig. 9(a)] with visible serrated edges at some regions of the steel's surface due to the action of RSZ which limits the effect of SO_4^{2-} ions on the steel.

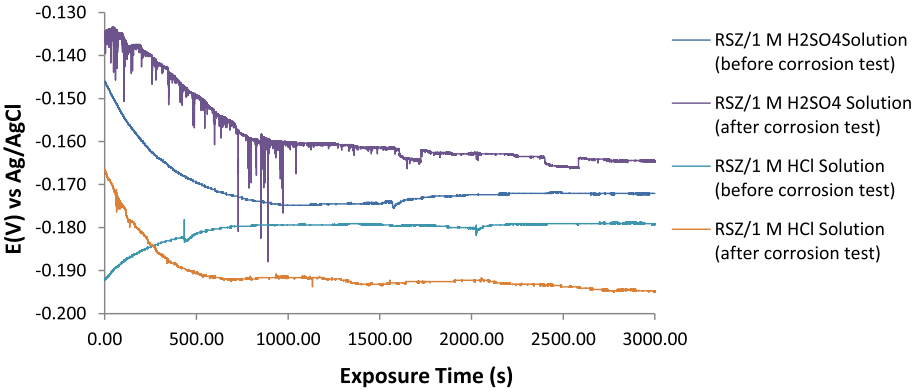

Fig. 6. Graphical plot of corrosion potential versus exposure time for LCS in 1 M HCl and H_2SO_4 solution.

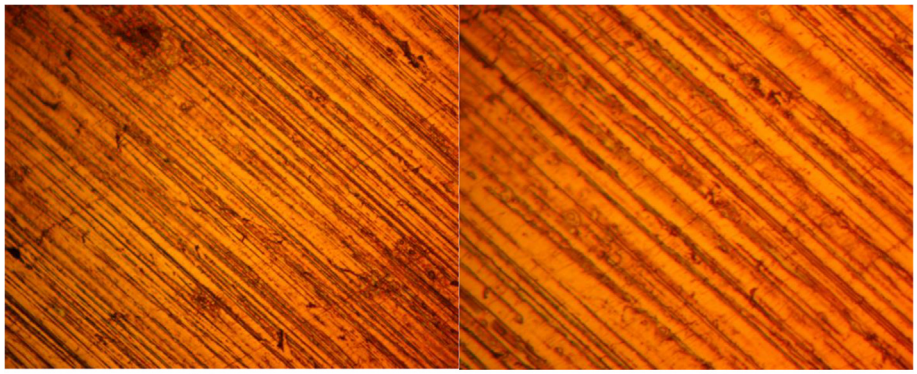

Fig. 7. Optical microscopy image of untested LCS specimen (a) mag. ×40, (b) mag. ×100.

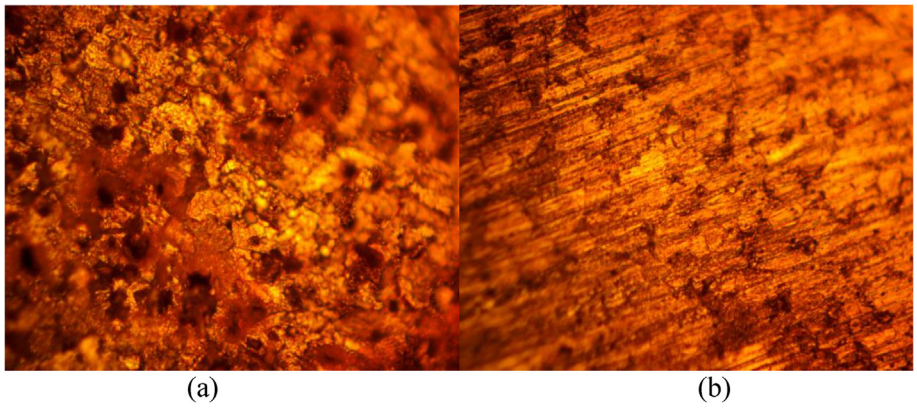

Fig. 8. Optical microscopy image of LCS specimen from HCl solution at mag. ×40 (a) corroded LCS, (b) RSZ inhibited LCS.

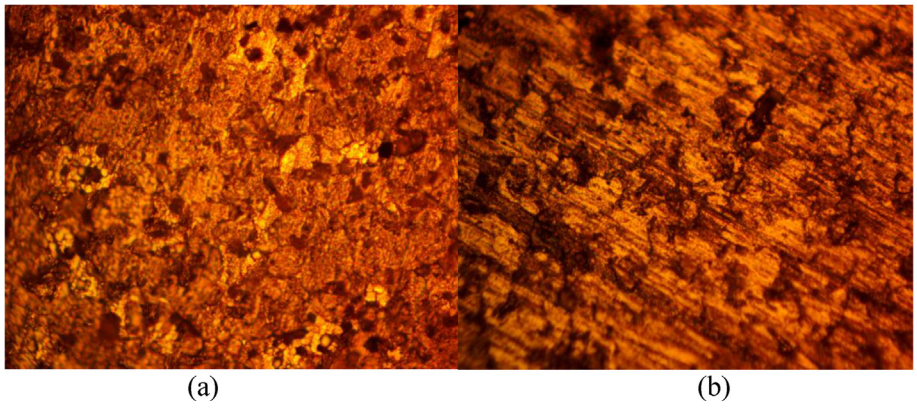

Fig. 9. Optical microscopy image of LCS specimen after H_2SO_4 solution at mag. ×40 (a) corroded LCS, (b) RSZ inhibited LCS.

Conclusion

The combined admixture of *Rosmarinus officinalis* and zinc oxide effectively inhibited the corrosion and surface oxidation of low carbon steel in dilute HCl and H_2SO_4 acid solution through surface coverage and selective precipitation. The compound performed more effectively in HCl solution from electrochemical analysis and corrosion potential monitoring. Adsorption onto the steel occurred through physisorption mechanism according to the Langmuir and Frumkin isotherm models. Identified functional groups completely adsorbed onto both steels from analysis of the adsorption spectra. The optical images of the inhibited steel specimens significantly contrast the images without the inhibiting compound due to the electrochemical action of the inhibitor cations on the inhibited steel which hindered the diffusion of corrosive anions onto the metal-inhibitor interface.

Acknowledgement

The author acknowledges Covenant University Ota, Ogun State, Nigeria for the sponsorship and provision of research facilities for this project.

Appendix A. Supplementary data

Supplementary data associated with this article can be found, in the online version, at https://doi.org/10.1016/j.rinp.2017.12.003.

References

[1] Yıldırım A, Çetin M. Synthesis and evaluation of new long alkyl side chain acetamide, isoxazolidine and isoxazoline derivatives as corrosion inhibitors. Corros Sci 2008;50(1):155–65.
[2] Gentil V. Corrosão. 4ª ed. Rio de Janeiro: LTC; 2003.
[3] Dariva CG, Galio AF. Developments in corrosion. In: Corrosion inhibitors – principles, mechanisms and applications. Intech Open; 2014. p. 366.
[4] Peter A, Obot IB, Sharma SK. Use of natural gums as green corrosion inhibitors: an overview. Int J Ind Chem 2015;6(3):153–64.
[5] Shi Mo S, Luo H-Q, Li N-B. Plant extracts as "green" corrosion inhibitors for steel in sulphuric acid. Chem Pap 2015;70(9). doi.org/10.1515/chempap-2016-0055.
[6] Souza EC, Ripper BA, Perrone D, Elia E. Roasted coffee extracts as corrosion inhibitors for mild steel in HCl solution. Mater Res 2016;19(6). doi.org/10.1590/1980-5373-mr-2015-0740.
[7] Gobara M, Zaghloul B, Baraka A, Elsayed M, Zorainy M, Mohamed Mokhtar Kotb MM, Elnabarawy H. Green corrosion inhibition of mild steel to aqueous sulfuric acid by the extract of *Corchorus olitorius* stems. Mater Res Express 2017;4. doi.org/10.1088/2053-1591/aa664a.
[8] Alvarez PE, Fiori-Bimbi MV, AdrianaNeske A, Brandán SASilvia A, Gervasi CA. *Rollinia occidentalis* extract as green corrosion inhibitor for carbon steel in HCl solution. J Ind Eng Chem 2017. doi.org/10.1016/j.jiec.2017.09.012.
[9] Bentiss F, Traisnel M, Lagrenee M. The substituted 1,3,4-oxadiazoles: a new class of corrosion inhibitors of mild steel in acidic media. Corros Sci 2000;42(1):127–34.
[10] Elkadi L, Mernari B, Traisnel M, Bentiss F, Lagrenee M. The inhibition action of 3,6-bis(2-methoxyphenyl)-1,2-dihydro-1,2,4,5-tetrazine on the corrosion of mild steel in acidic media. Corros Sci 2000;42(4):703–10.
[11] Kertit S, Hammouti B. Corrosion inhibition of iron in 1M HCl by 1-phenyl-5-mercapto-1,2,3,4-tetrazol. Appl Surf Sci 1996;93(1):59–66.
[12] Bentiss F, Lagrenee M, Traisnel M, Hornez JC. The corrosion inhibition of mild steel in acidic media by a new triazole derivative. Corros Sci 1999;41(4):789–95.
[13] Loto RT, Oghenerukewe E. Inhibition studies of *Rosmarinus Officinalis* on the pitting corrosion resistance 439ll ferritic stainless steel in dilute sulphuric acid. Orient J Chem 2016;32(5):2813–32.
[14] Loto RT. Corrosion inhibition performance of the synergistic effect of *Rosmarinus officinalis* and 5-bromovanillin on 1018 carbon steel in dilute acid media. J Fail Anal Prev 2017;17(5):1031–43.
[15] Klodian Xhanari K, Finšgar M, Hrnčiča MK, Uroš Maver U, Željko Kneza Z, Seiti B. Green corrosion inhibitors for aluminium and its alloys: a review. RSC Adv 2017;7(44):27299–330.
[16] Loto RT, Loto RO, Joseph OO, Akinwumi I. Electrochemical studies of the corrosion inhibition property of *Rosmarinus Officinalis* on mild steel in dilute sulphuric acid. J Chem Pharm Res 2015;7(7):105–16.
[17] Hasan SK. Rosemary extract as eco-friendly corrosion inhibitor for low carbon steel in 1 M HCl. J Ind Res Technol 2011;1(2):110–3.
[18] Abdallah M, Karanee Al SO, Fattah Abdel AA. Corrosion behavior of nickel andits alloys in HCl and its inhibition by natural rosemary oil. Zaštita Materijala 2009;50(4):205–12.
[19] Begum A. *Rosmarinus officinalis* L. herb as corrosion inhibitor for mild steel in sulphuric acid medium. Int J Pharm Sci Rev Res 2011;10(1):167–9.
[20] Vennilaa P, Kavithaa S, Venkateshb G, Madhua P. Experimental and theoretical investigation of Rosmarinus officinalis leaves extracts as the corrosion inhibitor for mild steel in H3PO4 solution; synergistic effect. Der Pharma Chemica 2015;7(5):275–83.
[21] El Ouariachi E, Paolini J, Bouklah M, Elidrissi A, Bouyanzer A, Hammouti B, Desjobert J-M, Costa J. Adsorption properties of *Rosmarinus officinalis* oil as green corrosion inhibitors on C38 steel in 0.5 M H_2SO_4. Acta Metall Sinica 2010;23(1):13–20.
[22] Kliškić M, Radošević J, Gudić S, Katalinić V. Aqueous extract of *Rosmarinus officinalis* L. as inhibitor of Al–Mg alloy corrosion in chloride solution. J Appl Electrochem 2000;30(7):823–30.
[23] Ameer MA, Fekry AM. Corrosion inhibition of mild steel by natural product compound. Prog Org Coat 2011;71(4):343–9.
[24] Loto CA, Joseph OO, Loto RT. Inhibition effect of zinc oxide on the electrochemical corrosion of mild steel reinforced concrete in 0.2 M H_2SO_4. J Mater Environ Sci 2016;7(3):915–25.
[25] Loto CA, Joseph OO, Loto RT, Popoola API. Effect of zinc oxide on the corrosion inhibition of mild steel embedded in concrete in 3.5% NaCl solution. Der Pharma Chemica 2015;7(12):85–96.
[26] Devi M, Kannan K. Evaluation of corrosion inhibition performance of zinc oxide and sodium nitrite in quarry dust concrete. Asian J Chem 2013;25(15):8690–6.
[27] Loto CA, Joseph OO, Loto RT. Effect of *Vernonia amygdalina* extract and zinc oxide inhibitor on the corrosion of mild steel reinforcement in concrete in 0.2 M H_2SO_4 environment. J Chem Pharm Res 2015;7(10):871–81.
[28] Munger CG, Vincent LD. Corrosion prevention by protective coatings. NACE; 1999.
[29] Brodd RJ, Leger VE, Bard AJ. In: Encyclopedia of electrochemistry of the elements. New York: Marcel Decker; 1976. p. 35.
[30] ASTM G1–03. Standard Practice for Preparing, Cleaning, and Evaluating Corrosion Test Specimens, http://www.astm.org/Standards/G1/; 2011 [Retrieved: 30/05/17].
[31] Ozcan MM, Chalchat JC. Chemical composition and antifungal activity of rosemary (*Rosmarinus officinalis* L.) oil from Turkey. Int J Food Sci Nutr 2008;9(7–8):691–8.
[32] ASTM G59–97. Standard Test Method for Conducting Potentiodynamic Polarization Resistance Measurements http://www.astm.org/Standards/G31/; 2014 [Retrieved: 30/05/17].
[33] ASTM G102 – 89. Standard Practice for Calculation of Corrosion Rates and Related Information from Electrochemical Measurements, http://www.astm.org/Standards/G31/; (2015)e1 [Retrieved: 30/05/17].
[34] Basics of corrosion measurements. http://www.che.sc.edu/faculty/popov/drbnp/ECHE789b/Corrosion%20Measurements.pdf/ [Retrieved: 06/04/17].
[35] ASTM G69 – 12 Standard test method for measurement of corrosion potentials of aluminum alloys, https://www.astm.org/Standards/G69.htm/ [Retrieved: 12/06/2017].
[36] Deyab MA, Keera ST, El Sabagh SM. Chlorhexidine digluconate as corrosion inhibitor for carbon steel dissolution in emulsified diesel fuel. Corros Sci 2011;53(8):2592–7.
[37] Riggs OL., Corrosion Inhibition, Nathan CC., 2nd ed., Houston, TX; 1973.
[38] Table of Characteristic IR Absorptions. http://orgchem.colorado.edu/Spectroscopy/specttutor/irchart.pdf [Retrieved: 12/01/2017].
[39] George S. Infrared and raman characteristic group frequencies: tables and charts. New York: John Wiley & Sons; 2004.
[40] Limousin G, Gaudet JP, Charlet L, Szenknect S, Barthes V, Krimissa M. Sorption isotherms: a review on physical bases, modeling and measurement. Appl Geochem 2007;22(2):249–75.
[41] Allen SJ, Mckay G, Porter JF. Adsorption isotherm models for basic dye adsorption by peat in single and binary component systems. J Colloid Interface Sci 2004;280(2):322–33.
[42] Bulut E, Ozacar M, Sengil IA. Adsorption of malachite green onto bentonite: equilibrium and kinetic studies and process design. Microporous Mesoporous Mater 2008;115(3):234–46.
[43] Guidelli R. Adsorption of molecules at metal electrodes. New York: VCH Publishers, Inc.,; 1992. p. 1.
[44] Hosseini M, Stijn FLM, Mohammed RA. Synergism and antagonism in mild steel corrosion inhibition by sodium dodecylbenzenesulphonate and hexamethylenetetramine. Corros Sci 2003;45(7):1473–89.
[45] Aharoni C, Ungarish M. Kinetics of activated chemisorption. Part 2. Theoretical models. J Chem Soc, Faraday Trans 1977;73:456–64.
[46] Loto RT, Loto CA, Joseph OO, Olanrewaju G. Adsorption and corrosion inhibition properties of thiocarbanilide on the electrochemical behavior of high carbon steel in dilute acid solutions. Results Phys 2016;6:305–14.
[47] Loto RT, Loto CA, Popoola API, Fedotova T. Inhibition effect of 2-amino-5-ethyl-1, 3, 4-thiadiazole on corrosion behaviour of austenitic stainless steel type 304 in dilute HCl solution. J Cent South Univ 2016;23:258–68.